International Journal of Nanoelectronics and Materials
IJNeaM
ISSN 1985-5761 | E-ISSN 2232-1535

A Study on Different Au Concentrations for A-Fe2O3@Au Hybrid Structure Preparation and Characterization

Hasan S. Jabbar[a], Evan T. Salim[a,*], Rana O. Mahdi[a], Iman H. Hadi[a], Subash C. B. Gopinath[b, c, d]

[a]*Collage of Applied Science, University of Technology-Iraq, Baghdad, Iraq*
[b]*Center for Global Health Research, Saveetha Medical College & Hospital, Saveetha Institute of Medical and Technical Sciences (SIMATS), Thandalam, Chennai – 602 105, Tamil Nadu, India*
[c]*Faculty of Chemical Engineering & Technology, Universiti Malaysia Perlis (UniMAP), 02600 Arau, Perlis, Malaysia*
[d]*Department of Technical Sciences, Western Caspian University, Baku AZ 1075, Azerbaijan*
[*]*Corresponding author. Tel.: h/p: +9647715752087; e-mail:evan.t.salim@uotechnology.edu.iq*

ABSTRACT

This research presents the effective synthesis of ferric oxide nanoparticles (Fe_2O_3) and α-Fe2O3 @Au hybrid structures in thin films at varying gold concentrations, utilizing the pulsed laser deposition (PLD) approach with a Nd:YAG laser. The creation of a nanohybrid was the outcome of depositing nano α-Fe_2O_3 with gold. The nanocomposite α-Fe_2O_3@Au, which has a hybrid structure, was the subject of characterization studies; XRD analysis confirmed the presence of polycrystalline nanoparticles with rhombohedral-centered hexagonal structures of Fe_2O_3, and the diffraction peaks for Au were indexed to the face-centered cubic phase of gold at orientation (64.5). The morphological properties were analyzed using Field Emission Scanning Electron Microscopy (FESEM), Atomic Force Microscopy (AFM), Energy-Dispersive X-ray Spectroscopy (EDX), as well as Ultraviolet-Visible (UV-Vis) analysis. According to the findings, the agglomerated nanoparticles of Fe_2O_3@Au have a spherical or semi-spherical shape and a tendency to form clumps. The hybrid structure of Fe_2O_3@Au also contains a higher concentration of agglomerated particles. The results indicated that particle sizes ranged from 166 to 505 nm, with an increase in gold content (Fe (III), O,79Au) correlating with a maximum particle size of 505 nm for pure α-Fe_2O_3. EDX analysis confirmed the presence of Fe and O components in the thin films. The optical analysis demonstrated that the samples possess an optical gap of around 2.6 eV, fluctuating with the substance's concentration variations.

KeyWord: *Ferric oxide (Fe_2O_3), Au-Fe_2O_3 hybridstructure, Pulse laser deposition , Structural properties, Morphological properties, Optical properties*

1. INTRODUCTION

Iron(III) oxide (Fe_2O_3) is a significant inorganic compound with diverse applications in industrial and scientific fields. It exists in several polymorphic forms, including (α-Fe_2O_3), (β-Fe_2O_3), (γ-Fe_2O_3), and (ε-Fe_2O_3), each possessing unique crystallographic structures and properties [1, 2]. The α-phase, known as hematite, is the most stable and naturally abundant form, featuring a rhombohedral structure. In contrast, the γ-phase, or maghemite, has a cubic structure and is metastable, often utilized in magnetic applications. The less common β and ε phases exhibit distinct magnetic and structural characteristics, with ε-Fe_2O_3 showing potential for high-density recording media due to its unique magnetic properties [3, 4].

In addition, magnetic nanoparticles have other benefits such as facile synthesis and functionalization, extensive surface area, limited toxicity, as well as cost-effectiveness (Maleki et al., 2018b, 2019b). Fe_2O_3 nanoparticles can be synthesized using various techniques, including microwave-assisted synthesis [5], thermal-decomposition [6, 7], chemical-method [8, 9], hydrothermal method [10, 11], co-precipitation method [12, 13], laser pyrolysis [14, 15], along with pulsed laser ablation, either in a vacuum [16, 17] or in a liquid environment [18, 19]. Pulsed laser ablation in liquid (PLAL) is an innovative technology for manufacturing hybrid structures.

This technique employs a high-power laser to ablate a bulk target material in a liquid solution, enabling the creation of nanostructures without chemical precursors or stabilizers. PLAL enables the size, structure, and composition of nanoparticles to be controlled with precision, making it a green and versatile method [20, 21].

Hybrid nanostructures have emerged as a significant area of research within nanotechnology, offering multifunctional materials with enhanced functionalities for numerous applications. of these, Au-Fe_2O_3 hybrid structures have received considerable interest due to the collective distinct optical, magnetic, and catalytic functionalities of their gold (Au) and iron oxide (Fe_2O_3) components [22, 23]. Owing to their relativistic effects, gold nanoparticles offer a platform for active metal-based nanocatalyst reactions for several organic transformation reactions. Gold catalysis has attracted huge attention after Haruta's landmark finding on the low-temperature oxidation of CO by Au nanoclusters [24, 25]. The higher stability of Au nanoparticles made them outperform other metal catalysts, such as Ru, Pd, Ag, and Pt, in their catalytic activity as well as selectivity [26-28].

Gold nanoparticles are known for their exceptional surface plasmon resonance (SPR), biocompatibility, and catalytic efficiency, while iron oxide exhibits remarkable magnetic properties and environmental remediation capabilities [29, 30]. Gold is a highly coveted substance, and hence, substantial quantities are regarded as quite precious. Its rarity, beautiful natural beauty, and distinctive physical and chemical qualities, especially its resistance to oxidation and corrosion, render gold a captivating and precious metal for several applications. A recent study has shown that minuscule quantities of gold can possess considerable value due to the novel and fascinating features that arise at the nanoscale [31, 32]. The surface functionalization of gold nanoparticles using diverse ligands leads to the formation of nanocomposites that demonstrate optical properties suitable for biological or medical applications [33, 34]. This includes advancements in ultrasensitive detection and imaging techniques, as well as enhancements in physical properties like magnetism [35, 36] and both linear and nonlinear optical characteristics [37]. It was demonstrated that the NLO activity of small metallic nanoparticles can be enhanced by deviation of the shape of the nanoparticles from a perfect sphere.This paper focuses on the synthesis of Au-Fe_2O_3 hybrid structures using pulsed laser ablation, highlighting their unique properties and structural characteristics.

2. EXPERIMENTAL WORK

Synthesized α-Fe_2O_3 @Au thin film nanoparticles by the target preparation technique involved α-Fe_2O_3 powder (sourced from US Research Nanomaterials, Inc.) with a purity of 96%, which was mixed with a gold solution at varying ratios. A total volume of 25 mL was prepared in a flask, incorporating a determined quantity of 10 mL of distilled water. The mixture of iron oxide and gold concentration was mixed for 24 hours. The physical mixing procedure is conducted using a magnetic stirrer device, followed by filtering using filter paper. Subsequently, 3 mg of the resultant powder was subjected to a pressure of 20 tons, yielding a cylindrical pellet with a diameter of 2 cm and a height of 0.5 cm, depicted in Figure 1.

The gold solution was synthesized employing pulsed laser ablation in liquid using a Nd:YAG laser (1064 nm), extracting nanoparticles from a gold target in distilled water. Various concentrations of gold solution were formulated under conditions of 500 mJ and 700 mJ, maintaining a constant pulse count of 450 pulses. Sample (1) consists of pure α-Fe_2O_3 nanoparticles, whereas sample (2) is α-Fe_2O_3@Au synthesized in a gold solution using a laser energy of 500 mJ. Sample (3) is α-Fe_2O_3@Au created with a gold concentration utilizing a laser energy of 700 mJ. Subsequently, synthesize α-Fe_2O_3 @Au nano-thin films utilizing the pulsed laser deposition (PLD) technique with a Nd:YAG laser (1064 nm) through these samples. Laser energy of 500 mJ per 150 pulses under a vacuum of 2 x 10^-8 mbar and at a temperature of 100°C. While XRD studies were used to explain the structural characteristics of α-Fe2O3 thin films, a UV-visible spectrophotometer was used to analyze their optical properties. The topographies of the films were investigated with AFM, and the surface morphologies were studied with FE-SEM. The elemental compositions were also ascertained by the use of EDX analyses. The PLD method was used to carry out the deposition testing. The PLD system uses a Q-switched Nd:YAG pulsed laser (HF-301, Huafei Technology, China), which can be seen in Figure 1. A distance of 6 cm separated the target surface from the laser head. The distance between the substrate and the target was around 4 cm. A 12 cm focal length convex lens was used to focus the laser beam.

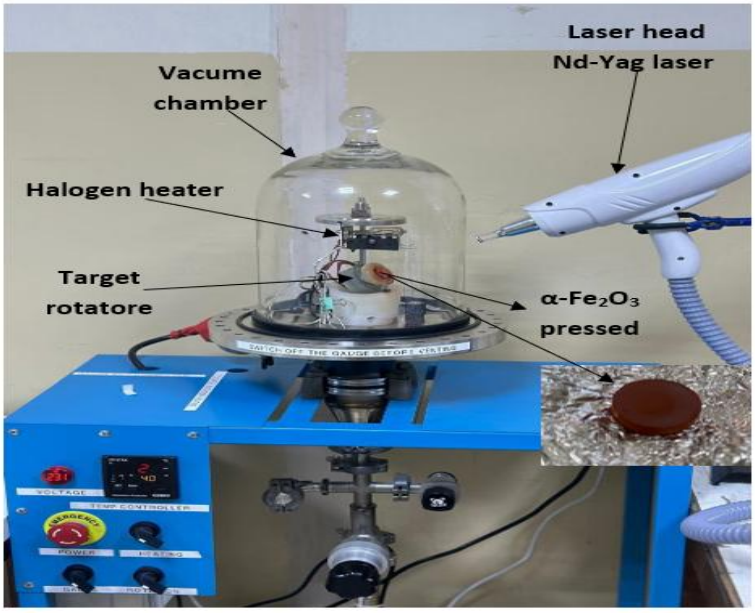

Figure 1. Pulsed laser deposition (PLD) system.

3. RESULT AND DISCUSSION

3.1 Structural Properties of Fe2O3 with Au

3.1.1 X-Ray Diffraction (XRD)

This technique is utilized to determine the molecular and atomic configuration of a crystal and to detect any crystalline irregularities. This approach can be utilized on a diverse array of materials, including metals, semiconductors, salts, organic and inorganic substances, as well as biological molecules. XRD was utilized to obtain essential information regarding average grain size, structural strain, along with the presence of impurities.

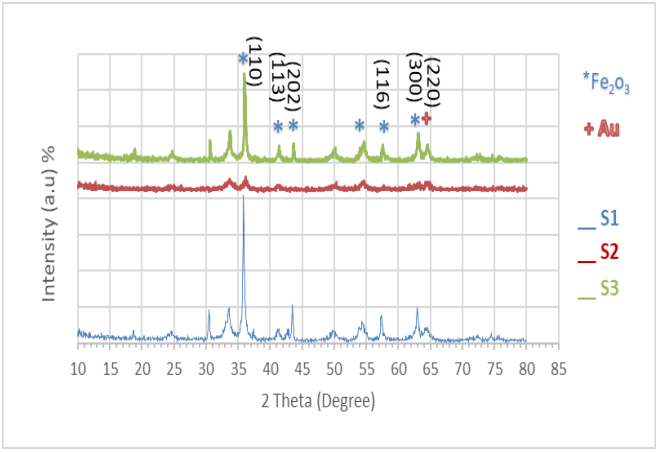

Figure 2. The patterns of XRD for α-Fe_2O_3 and the α-Fe_2O_3@Au with different laser energy.

Figure 2 displays the patterns of XRD diffraction patterns of α-Fe_2O_3 nanostructure and α-Fe_2O_3 hybrid structure nanocomposite. The diffraction peaks for α-Fe_2O_3 are observed at 33.5, 35.8, 43.5, 49.7, 54.1, 57.35, and 63.1, with indices (104), (110), (202), (024), (116), (122), and (300). This pertains to a rhombohedral-centered hexagonal structure of corundum type, distinguished by a densely packed oxygen lattice with two-thirds of the octahedral sites filled by Fe(III) ions, under the documented XRD data (JCPDS File No. 87-1166). The obtained XRD images of the α-Fe_2O_3@Au nanohybrid were analyzed by comparing them with the resulting patterns of α-Fe_2O_3 and Au. After the mixing process, under the conditions of 500 mJ and 450 pulses, X-ray diffraction of the α-Fe_2O_3@Au target reveals peaks at 2θ = 33.6, 36.2, 41.5, 50.3, 54.55, 57.75, and 64.7, corresponding to orientations (104), (110), (113), (024), (116), (018), and (220), indicative of a hexagonal configuration for α-Fe_2O_3@Au (JCPDS Card No. 86–0550). All peaks corresponding to α-Fe_2O_3 were seen, including a notable peak at 64.7. The diffraction peak for Au in the nanocomposite aligns with [JCPDS File No. 89-3697]. The target was fabricated under circumstances of 700 mJ and 450 pulses of Nd: YAG laser. The diffraction peaks for the synthesized α-Fe_2O_3@Au at varying laser energies exhibited peaks at 2θ = 33.7, 36, 41.42, 43.65, 50.5, 54.7, 63.1, and 64.5, corresponding to indices (104), (110), (113), (202), (024), (116), (300), and (220), respectively, indicating a thin mixture of α-Fe_2O_3 with gold. All the peaks observed are attributed to Fe_2O_3, except for the peak at 64.5, which corresponds to Au. According to JCPDS File No. 89-3697, the peak values of diffraction for Au in the nanocomposite are associated with the face-centered cubic phase of gold. Furthermore, the X-ray results can be correlated with the search outcomes [38, 39]. Table 1 displays the grain sizes, dislocation densities, Miller indices, as well as microstrains of α-Fe_2O_3@Au nanoparticles produced using different laser energy levels. Scherrer's formula was employed to ascertain the crystallite size (D) [40-42].

$$D=(0.9\,\lambda)/(\beta\ COS(\theta)) \quad (1)$$

Where the constant k is presumed to be 0.94, λ represents the employed X-ray wavelength, thought to be 1.54 Å, and θ denotes the full width at half maximum of the X-ray diffraction pattern, equivalent to Bragg's angle.

To compute the strain (ε) as well as dislocation density (δ) of the Fe_2O_3 nanoparticle, the subsequent equations were employed [43-45]:

$$\delta= 1/D\text{^}2 \quad (2)$$

Lattice strain arises from lattice flaws, including dislocations, vacancies, interstitials, along with substitutional defects. This strain can be calculated using the equation shown below [46-48]:

$$\eta= (\beta\ )/(4\ \tan\theta\ ) \quad (3)$$

The incorporation of gold (Au) into iron oxide (Fe_2O_3) significantly affects its crystal lattice structure. Due to the considerable difference in atomic radii between Au (0.144 nm) and Fe (0.124 nm), internal lattice strain is introduced, leading to distortions in the Fe_2O_3 lattice and shifts in the X-ray diffraction (XRD) peaks [49, 50]. Additionally, Au nanoparticles act as nucleation sites during the crystallization process, thus modifying the grain size, often resulting in larger crystallite sizes depending on the

synthesis conditions [51, 52]. Gold also influences the phase stability of Fe_2O_3, favoring the stabilization of the hematite phase (α-Fe_2O_3) or promoting phase transitions depending on surface energy alterations [53, 54].

Table 1 Miller indices, crystalline size, dislocation density, and microstrains of the orthorhombic α-Fe2O3@Au nanoparticles

2θ	FWHM	Miller indices	Crystalline size(nm)	Dislocation density(δ) lines. m-2	Microstrains (η)
33.7	0.37	104	2.65	0.37	0.09
36	0.25	110	2.48	0.40	0.06
41.42	0.26	113	2.17	0.46	0.06
43.65	0.22	202	2.07	0.48	0.05
50.5	0.36	024	1.80	0.55	0.09
54.7	0.20	116	1.68	0.59	0.05
63.1	0.33	300	1.47	0.68	0.08
64.5	0.27	220	1.44	0.69	0.06

3.1.2 Energy Dispersive X-ray Spectroscopy (EDX)

A method employed for the analysis of elemental composition of materials. The data of EDX illustrates the peaks corresponding to the x-ray energy levels with the highest exposure. The ionization of atoms by high-energy radiation, resulting in the removal of inner shell electrons, generates the characteristic features of X-rays [55, 56]. The energy-dispersive X-ray spectroscopy (EDX) results for iron oxide nanoparticles and the synthesis of Fe2O3 @Au were obtained using a 1064 nm Nd:YAG laser with an energy range of 500-700 mJ per 450 pulses. As demonstrated in Figure 3, these targets were prepared for EDX examination by mixing iron oxide (Fe_2O_3) with gold (Au) using a magnetic stirrer device. Table 2 represents wt% of sample elements and stoichiometries of Fe_2O_3.

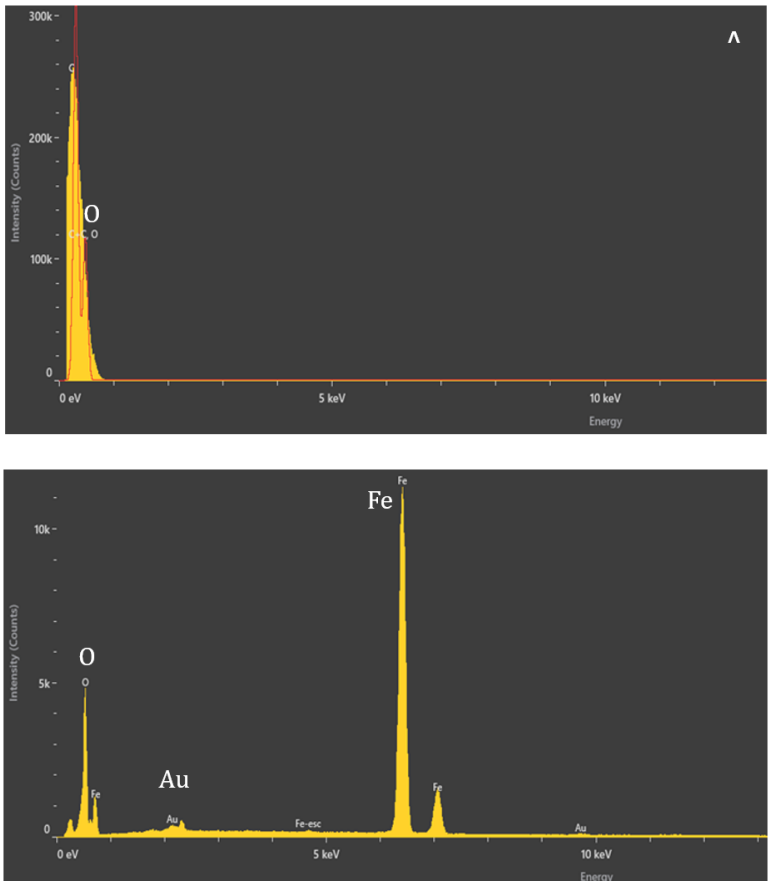

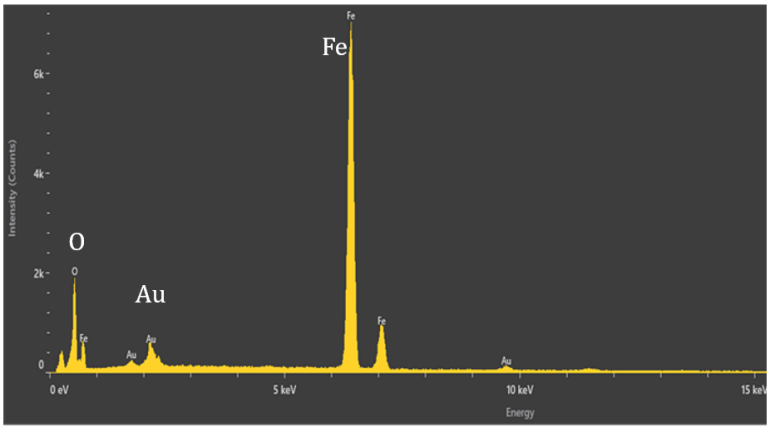

Figure 3. EDX Spectrum of the A- pure α-Fe2O3 NPs , B- α-Fe2O3 @Au at 500 mj , C- α-Fe2O3 @Au at 700 mj.

Table 2 Weight percentages and stoichiometries of Fe2O3 nanoparticles synthesized using different laser energies.

Laser energy (mj)	Au wt%	Fe wt%	O wt%	Fe2O3@Au Stoichiometry
pure		**79.8**	**20.2**	1.6
500mj	**1.8**	**72.2**	**25.9**	1.2
700mj	**5.3**	**76.0**	**18.7**	1.74

3.2 Synthesis Thin Films of α-Fe2O3@Au

3.2.1 X-Ray Diffraction Thin Films (XRD)

Pulsed laser deposition (PLD) is a physical vapor deposition technique that uses a Nd:YAG laser (1064 nm) with an energy of 500 mJ per 500 pulses to deposit a nanomaterial in a thin film. The X-ray diffraction patterns obtained from this process were used to characterize the deposited thin films structurally. The films were deposited on a silicon p-type (100) wafer.

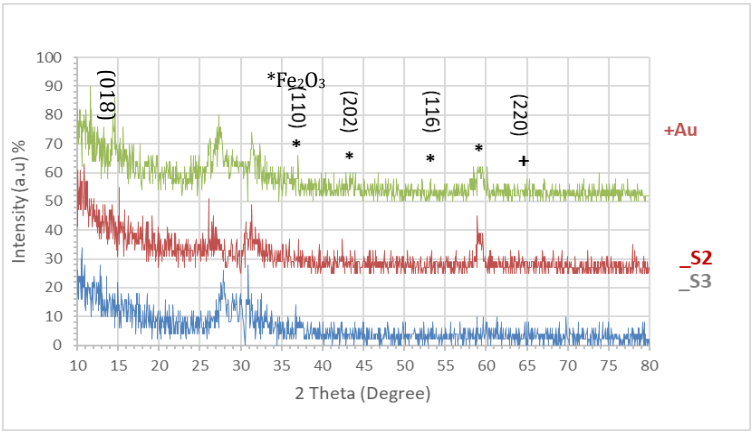

Figure 4. XRD diffraction patterns of α-Fe2O3 nanostructure as well as α-Fe2O3 @Au with different laser energy thin film nanostructure.

Figure 4 displays the patterns of XRD for α-Fe2O3 as well as α-Fe_2O_3@Au (hybrid structure) thin film nanocomposite. The X-ray diffraction analysis revealed principal peaks corresponding to the diffraction planes of the α-Fe_2O_3@Au nanohybrid, identified by comparison with the patterns of α-Fe_2O_3 and Au. The peaks observed at 2θ = 35.8°, 42.2°, 52.9°, 58.9°, and 64.8° correspond to indices (110), (202), (116), (018), and (220), indicating that the α-Fe_2O_3@Au possesses a hexagonal configuration (JCPDS Card No. 86 0550). All of the peaks following for α-Fe2O3 and except the (64.8). The XRD patterns also confirm the presence of elemental Au and show peaks from the face-centered cubic phase of gold (JCPDS File No.89 3697) with reflections from the (220) planes. The peak of gold increases with the increase in gold concentration, and the occurrence of the gold particles can create lattice strain, leading to shifts in the peaks observed in XRD patterns for iron oxide. This is a result of changes in the interatomic distances due to the presence of a foreign element in the materials [57, 58].

3.2.2 Field Emission Scanning Electron Microscopy (FESEM)

Field emission scanning electron microscopy (FESEM) was used to examine the structural morphology of the α-Fe2O3@Au hybrid structure that was created using pulsed laser deposition (PLD). Illustrated the FESEM picture of hematite nanoparticles synthesized by a hybrid structure incorporating iron oxide α-Fe_2O_3 and gold concentration (Au). Figure 5-a presents FESEM observations indicating the presence of (α-Fe_2O_3) nanoparticles. The SEM image reveals that the nanoparticles are uniformly dispersed, spherical, homogeneous, and consist of agglomerated tiny particles [59, 60]. The average size of the pure Fe_2O_3 is found to be about 34 nanometers and was calculated by the IMAGE-J software. Figure 5-b shows the surface morphology of the α-Fe_2O_3 @Au sample 1 of the particles; The typical particle size is 20 nanometers, and it contains small, clumped spherical particles. Figure 5-c shows synthesized α-Fe_2O_3@Au in sample 2. Particles agglomerate showed at 700 mJ laser energy. NPs are discovered to be spherical and interconnected. As the laser fluence is further increased, larger spherical particle formations are generated. catalyst reveals that the nanoparticles increased with increasing laser energy [55, 61]. The average size of α-Fe_2O_3@Au when increasing the gold concentration nanoparticle was found to be 60 nanometers. The outcome is dependable in conjunction with the EDX analysis results of the prepared sample. The outcome is dependable in conjunction with the EDX analysis results of the prepared sample.

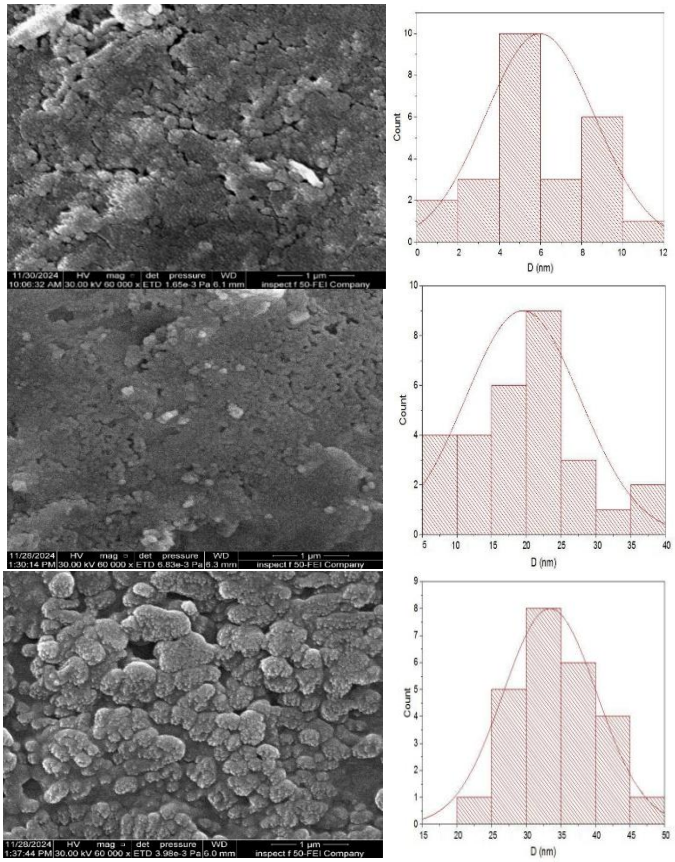

Figure 5. FESEM image of (a) Fe_2O_3 nanoparticles, (b)&(c)Fe_2O_3 @Au hybrid structure prepared by different laser energy.

3.2.3 Energy Dispersive X-ray Spectroscopy (EDX)

EDX results for Fe2O3 nanoparticles that were prepared by pulsed laser deposition technique by targets from Fe_2O_3 and Fe_2O_3@Au with different laser energies, where the thin films were prepared under conditions of 500 mJ per 150 pulses under a vacuum using a 1064 nm Nd:YAG laser. Three samples of Fe_2O_3 and Fe_2O_3@Au hybridized with gold were prepared on quartz glass. Figure 6 verifies the existence of iron, oxygen, gold, and carbon. Table 3 illustrates the weight percentage of sample elements and the stoichiometries of Fe_2O_3@Au.

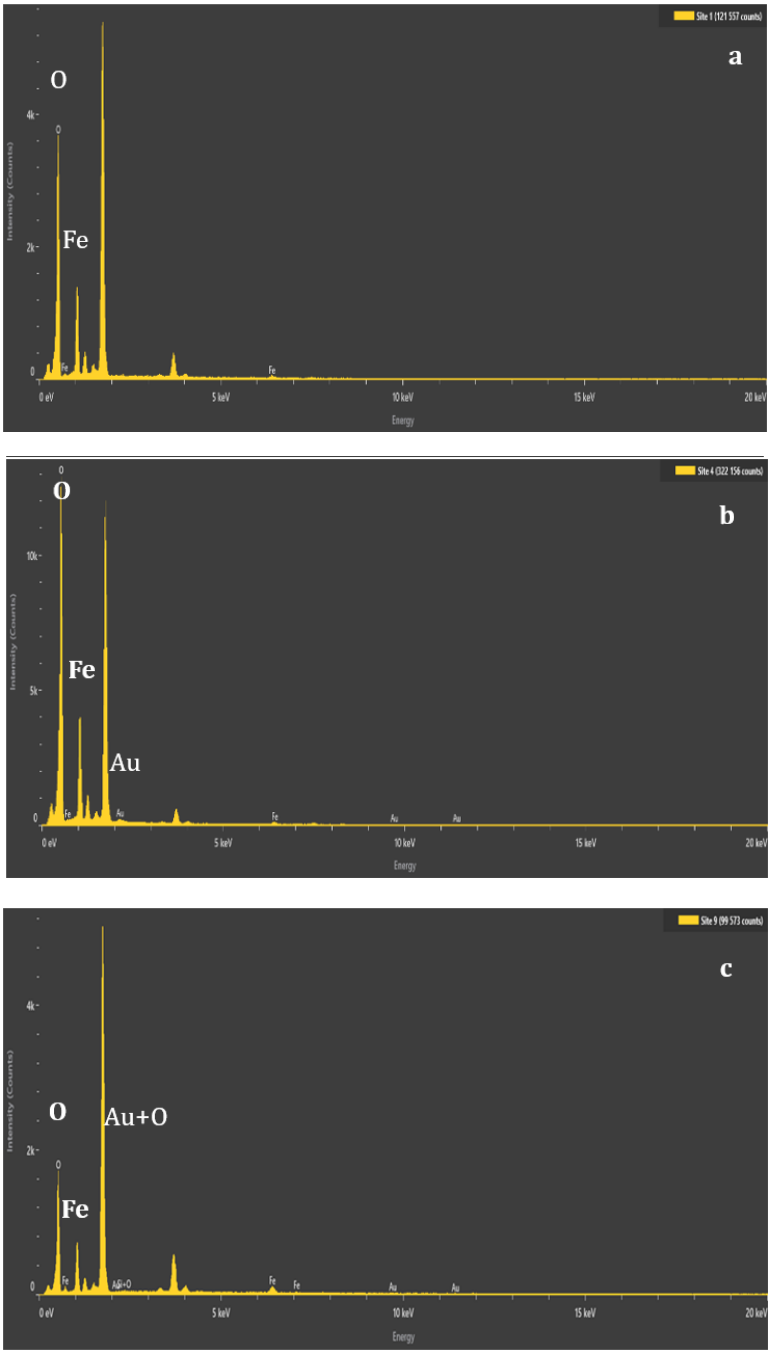

Figure 6. EDX spectrum of the prepared thin film when a) pure α-Fe2O3 NPs b) α-Fe2O3 @Au at 500 mj c) α-Fe2O3 @Au at 700 mj.

Table 3 Weight percentages and stoichiometries of elements in Fe_2O_3 thin film nanoparticles synthesized using different laser energy levels

Laser energy (mJ/Pulse)	Average particle size (nm)	Roughness (nm)	(RMS) (nm)
Pure	225.5	5.710	8.284
500	166.7	5.517	7.928
700	505.0	5.036	6.906

3.2.4 Atomic Force Microscopy (AFM)

Atomic force microscopy (AFM) was also used to investigate the surface morphology and roughness of α-Fe_2O_3 nanoparticles. Figure 7 shows the two-dimensional (2D), three-three-dimensional (3D) image spherical shape for the α-Fe_2O_3 nanoparticles prepared by samples for fig 7-a of pure α-Fe_2O_3 to sample (1) and Figure 7-b of α-Fe_2O_3@Au to sample 2 at 500 mj, and Figure 7-c of α-Fe_2O_3@Au at 700 mj sample 3, furthermore, the creation of semi-spherical clusters occurs with agglomeration particle sizes (aggregate grains). Table 4 shows that for different laser energies, the average particle size, surface roughness, and root mean square of iron oxide nanoparticles are displayed, where the average particle size increases and decreases in surface roughness and root mean square (RMS). Thin film layers are grown during deposition by interacting with ablation products in the plasma, resulting in grain size purification due to secondary laser deposition at elevated laser energy, which subsequently increases the grain size.

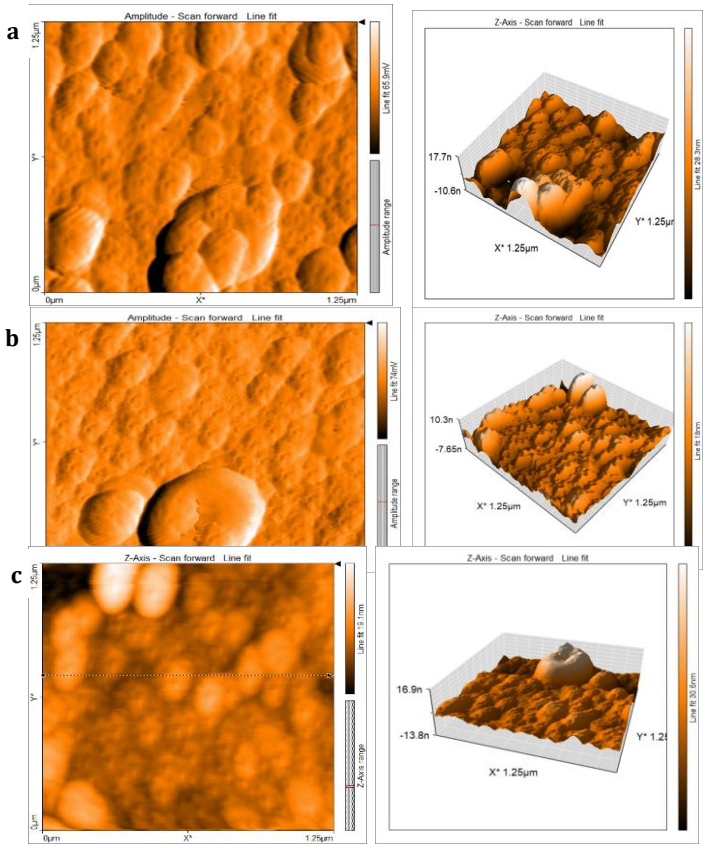

Figure 7. AFM image 2D and 3D distribution topgraphical of (a)pure α-Fe_2O_3 (b) α-Fe_2O_3 @Au at 500 mj (c) α-Fe_2O_3 @Au at 700 mj.

Table 4 Average particle size, roughness, along with RMS values of the prepared α-Fe_2O_3 @Au nanoparticle thin films.

Laser Energy mJ	Au wt%	Fe wt%	O wt%	Fe_2O_3@Au Stoichiometry
pure		**2.1**	**97.9**	0.009
500	**1.2**	**1.6**	**97.2**	0.007
700	**1.7**	**5.5**	**92.7**	0.025

Figure 6 displays topographical examinations of the surface of α-Fe_2O_3@Au nanoparticles. AFM data indicated a rise in the average particle size, ranging from 166 to 505 nm, while roughness reduced, measuring between 5.710 and 5.036. Similarly, the root mean square roughness ranged from 8.284 to 6.906 nm. These findings corroborate those of other previously reported studies [62, 63].

3.3 Optical Properties

3.3.1 UV-Visible Measurements

The optical absorption spectrum and characteristics of the α-Fe_2O_3 nanoparticles were observed in Figure 8 within the wavelength range of 190-900 nm. The UV absorption efficacy of finished textiles demonstrated superior results in comparison to control samples. When α-Fe2O3 nanoparticles are ablated from a larger surface area, their band gap energy rises.

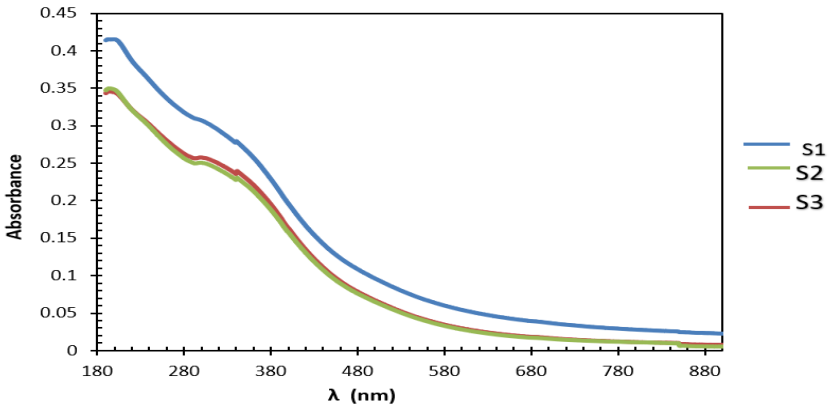

Figure 8. Absorption spectrum of α-Fe_2O_3@Au thin films prepared by PLD at various energies of laser.

By visually utilizing Tauc's formula [64-66], the optical band gap (Eg) for direct transition can be ascertained:

$$(\alpha h\nu)^2=A^2 (\lambda\nu\_ Eg) \quad (4)$$

In which A is a constant, α is the absorption coefficient, hυ is the photon energy of incident light, and Eg represents the optical energy gap. The absorption spectra and direct band gaps of α-Fe_2O_3 nanoparticles synthesized employing a variety of laser energies ranging from 500 to 700 mJ. The energy gap, illustrated in Figures 9-a, b, c and Table 5 below, increases with the rise in laser energy, attributed to the augmentation of the thin film's thickness, which results from the elevation of localised energy levels among the bands of conduction and valence.[67, 68] The figure shows that the absorbance spectra were red-shifted as the laser intensity increased, which is indicative of both a higher concentration of the ablated material and larger particles. The direct band gap values were calculated using equation 4, where A is a constant, h is the photon energy, and Eg is the optical band gap energy. Eg can be observed from the extrapolation of the Tauc plot when the curve $(\alpha h\upsilon)^2$ [53, 69]. The direct band gap of α-Fe_2O_3 nanoparticles prepared using different ranges of laser energy. Moreover, the band gap values are augmented with the rise in laser energy. This is because, as previously mentioned, the band gap value is decreased under a weak confinement regime, and the size of the nanoparticles reaches a level greater than the exciton Bohr radius value [62, 70]. These findings corroborate the findings of the XRD and FESEM analyses discussed earlier in this study. The Au nanoparticles significantly enhance absorption due to the Au plasmon absorption band. Despite the seeds exhibiting a feeble plasmon resonance, absorbance significantly escalates, accompanied by a red shift as Au nanoparticles aggregate on the α-Fe_2O_3 surface due to enhanced particle size and interparticle interactions [71, 72]. In 2013, Gobinda Gopal Khan et al. discovered that the photoluminescence (PL) properties of semiconductor nanostructures and nanowires (NWs) are significantly improved by surface plasmon resonance (SPR) by the deposition of noble metals like Au or Pd on their surfaces.[73-75] Furthermore, recent findings indicate that the magnetism of ferromagnetic oxide nanostructures can be enhanced by several orders of magnitude via surface modification with a gold coating In this context, semiconductor magnetic nanostructures, enveloped by nonmagnetic metallic materials, may exhibit remarkable optical and magnetic capabilities simultaneously, Therefore, it is anticipated that the deposition of a noble metal such as Au on the surface of α-Fe_2O_3 NWs can effectively modify their luminescent and magnetic characteristics. [76, 77]

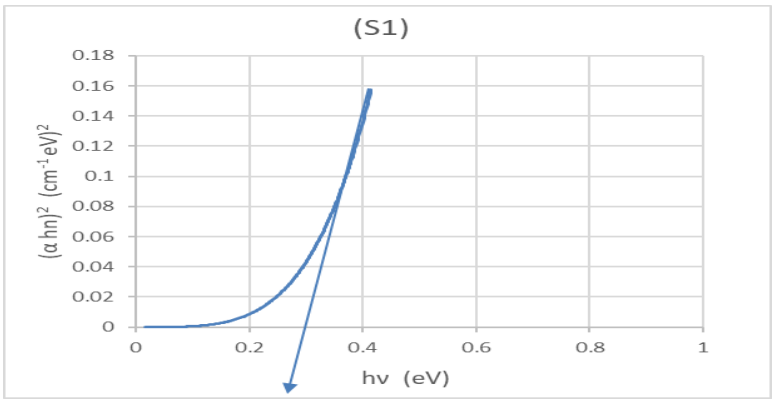

Figure 9-c. plot of (αhυ)2 versus (hυ) of S1.

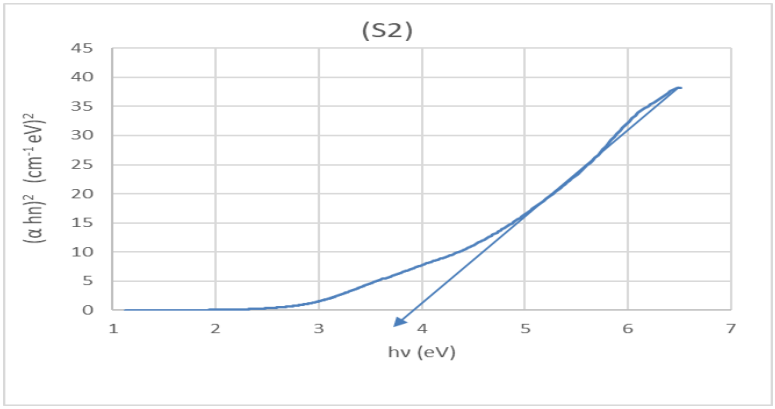

Figure 9-c. Plot of (αhυ)2 versus (hυ) of S2.

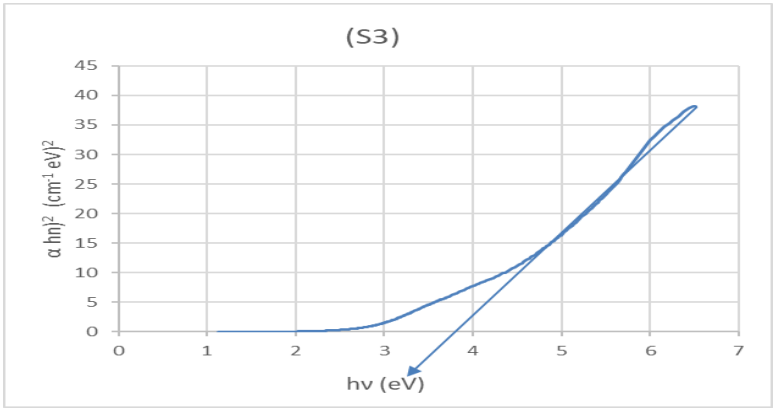

Figure 10-c. Plot of (αhυ)2 versus (hυ) of S3.

Table 5 Band Gap Energy of α-Fe_2O_3 @Au

Laser energy (mJ/Pulse)	Energy gap (e.v)
Sample 1	2.8
Sample 2	3.9
Sample 3	3.8

4. CONCLUSION

α-Fe_2O_3 thin film nanoparticles were effectively produced using the pulsed laser deposition approach at varying energies. Both XRD and FESEM analyses corroborate the existence of α-Fe_2O_3 and elemental Au. The crystallite sizes of the powders derived from XRD and FESEM are congruent. The results demonstrated that an increase in laser energy correlates with an increase in particle size, resulting in a blue shift in absorption spectra, broadening the optical energy gap. As the energy gap increases, the number of charged carriers escalates, so improving conductivity while reducing mobility, resistance, as well as Hall voltage. The XRD measurements confirmed the high purity of the α-Fe_2O_3 phase.

REFERENCE

[1] Zboril, R., Mashlan, M., & Petridis, D. (2002). Polymorphous transformations of nanometric iron(III) oxide: A review. Chemistry of Materials, 14(3), 969–982.

[2] Salih, E. Y. (2024). Opto-electrical evaluation of visible blind fast-response nanostructured SnO 2/Si photodetector. RSC advances, 14(38), 27733-27740.

[3] Dejoie, C., Tamura, N., Kunz, M., & Nishimura, T. (2015). Learning from the past: Rare ε-Fe_2O_3 in the ancient black-glazed Jian (Tenmoku) wares. Scientific Reports, 5, 15091.

[4] Hashim, A. H., Jasim, O. Z., Salih, M. M., The Establishing of Geospatial Database for Agricultural Lands of Islamic WAQF in Iraq: Case Study Babil Province, IOP Conference Series: Earth and Environmental ScienceThis link is disabled., 2022, 961(1), 012025.

[5] T. A. Lastovina, A. P. Budnyk, M. A. Soldatov, Y. V. Rusalev, A. A. Guda, A. S. Bogdan and A. V. Soldatov, "Microwave-assisted synthesis of magnetic iron oxide nanoparticles in oleylamine– oleic acid solutions," Mendeleev Commun., vol. 27, no. 5, pp. 487–489, 2017.

[6] Salih, E. Y. (2024). Fabrication of CdSe/Si nanostructure for self-powered visible light photodetector. Materials Letters, 371, 136930.

[7] A. Lassenberger, A. Lassenberger, T. A. Gr newald,P. D. J. van Oostrum, H. Rennhofer, H. Amenitsch, R. Zirbs, H. C. Lichtenegger and E. Reimhult, "Monodisperse Iron Oxide Nanoparticles by Thermal Decomposition: Elucidating Particle Formation by Second-Resolved in Situ Small-Angle X-ray Scattering," Chem. Mater., vol. 29, no. 10, pp. 4511–4522, 2017.

[8] Salih, E. Y. (2024). Fabrication and photodetection performance evaluation of nanostructured CdS/Si MSM visible light photodetector. Optical Materials, 149, 115120.

[9] J. B. Mamani, L. F. Gamarra, and G. E. de S. Brito, "Synthesis and characterization of Fe3O4 nanoparticles with perspectives in biomedical applications," Mater. Res., vol. 17, no. 3, pp. 542– 549, 2014.

[10] Alakrach, A. M., Noriman, N. Z., Dahham, O. S., Hamzah, R., Alsaadi, M. A., Shayfull, Z., & Syed Idrus, S. Z. (2018, June). The Effects of Tensile Properties of PLA/HNTs-ZrO2Bionanocomposites. In Journal of Physics: Conference Series (Vol. 1019, p. 012066). IOP Publishing.

[11] Dahham, O. S., & Zulkepli, N. N. (2020). Robust interface on ENR-50/TiO2 nanohybrid material based sol-gel technique: insights into synthesis, characterization and applications in optical. Arabian Journal of Chemistry, 13(8), 6568-6579.

[12] H. Hayashi and Y. Hakuta, "Hydrothermal Synthesis of metal oxide nanoparticles in supercritical water," Materials (Basel)., vol. 3, no. 7, pp. 3794–3817, 2010.

[13] Dahham, O. S., Noriman, N. Z., Sam, S. T., Rosniza, H., Marwa, N. A. S., Shayfull, Z., & Alakrach, A. M. (2016). The effects of trans-polyoctylene rubber (TOR) as a compatibilizer on the properties of epoxidized natural rubber/recycled silicone catheter (ENR-25/rSC) Vulcanizate. In MATEC Web of Conferences (Vol. 78, p. 01076). EDP Sciences.

[14] P. L. Hariani, M. Faizal, R. Ridwan, M. Marsi, and D. Setiabudidaya, "Synthesis and Properties of Fe3O4 Nanoparticles by Co-precipitation Method to Removal Procion Dye," Int. J. Environ. Sci. Dev., vol. 4, no. 3, pp. 336–340, 2013.

[15] Mohammed, M., Rozyanty, R., Mohammed, A. M., Osman, A. F., Adam, T., Dahham, O. S., ... & Betar, B. O. (2018). Fabrication and characterization of zinc oxide nanoparticle-treated kenaf polymer composites for weather resistance based on a solar UV radiation. BioResources, 13(3), 6480-6496.

[16] R. Alexandrescu, V. Bello, V. Bouzas, R. Costo, and F. Dumitrache, "Iron Oxide Materials Produced by Laser Pyrolysis," pp. 22–25, 2010.

[17] Hassanain Al-Taiy, Proposed Photonic Integrated Circuit For Photonic Networks, Engineering and Technology Journal, 28(8), 1567-1580 (2010).

[18] Mohammed M. Hameed, Abdul-Majeed E. Al-Samarai and Kadhim A. Aadim, "Synthesis and Characterization of Gallium Oxide Nanoparticles using Pulsed Laser Deposition" Iraqi Journal of Science, 2020, Vol. 61, No. 10, pp: 2582-2589.

[19] Stefan Preussler, Hassanain Al-Taiy, and Thomas Schneider, Generation and Stabilization of THz-waves with Extraordinary Low Line Width and Phase Noise, CLEO: 2015, OSA Technical Digest (online) (Optica Publishing Group, 2015),paper STu4H.6, https://doi.org/10.1364/CLEO_SI.2015.STu4H.6.

[20] K. S. Khashan, G. M. Sulaiman, and R. Mahdi, "Preparation of iron oxide nanoparticles decorated carbon nanotube using laser ablation in liquid and their antimicrobial activity," Artif. Cells, Nanomedicine, Biotechnol., vol. 1401, no. February, pp. 1–11, 2017.

[21] Fakhri M. A.; Salim E. T.; Wahid M. H.A. ; Salim Z. T.; Hashim U., A novel parameter effects on optical properties of the LiNbO3 films using sol-gel method, AIP Conference Proceedings, 2213, 20242 (2020) 10.1063/5.0000206.

[22] Zhang, J., Wang, X., & Zhou, Y. (2018). Synergistic optical and magnetic properties of Au-Fe_2O_3 hybrid nanostructures for catalytic and biomedical applications. Journal of Materials Chemistry C, 6(23), 6352-6360.

[23] Jehan A. Saimon, Suzan N. Madhat, Khawla S. Khashan, Azhar I. Hassan, Rana O. Mahdi, Rafah A. Nasif, Synthesis of CdxZn1-xO nanostructure films using pulsed laser deposition technique, AIP Conf. Proc. 2045, 020003 (2018) https://doi.org/10.1063/1.5080816.

[24] Fakhri M. A.; Bader B. A.; Khalid F. G.; Numan N. H.; Abdulwahhab A. W.; Hashim U.; Salim E. T.; Munshid M. A.; Salim Z. T., Optical and morphological studies of LiNbO3 nano and micro photonic structural, AIP Conference Proceedings, 2045, 20017 (2018) 10.1063/1.5080830.

[25] Bao, Y., Chen, Z., & Liu, T. (2016). Au-Fe_2O_3 hybrid nanostructures: Synthesis, properties, and applications. Chemical Society Reviews, 45(12), 3988-4016.

[26] Muhsien M. A.; Salem E. T.; Agool I. R.; Hamdan H. H., Gas sensing of Au/n-SnO2/p-PSi/c-Si heterojunction devices prepared by rapid thermal oxidation, Applied Nanoscience (Switzerland), 4(6), 719-732 (2014) 10.1007/s13204-013-0244-7.

[27] Daniel, M.-C.; Astruc, D. Gold Nanoparticles: Assembly, Supramolecular Chemistry, Quantum-Size-Related Properties, and Applications toward Biology, Catalysis, and Nanotechnology. Chem. Rev. 2004, 104, 293-346.

[28] Fakhri M. A.; Numan N. H.; Mohammed Q. Q.; Abdulla M. S.; Hassan O. S.; Abduljabar S. A.; Ahmed A. A., Responsivity and response time of nano silver oxide on silicon heterojunction detector, International Journal of Nanoelectronics and Materials, 11(Special Issue BOND21), 109-114 (2018).

[29] Saha, K.; Agasti, S. S.; Kim, C.; Li, X.; Rotello, V. M. Gold Nanoparticles in Chemical and Biological Sensing. Chem. Rev. 2012, 112, 2739-2779.

[30] Salata, O.V. Applications of nanoparticles in biology and medicine. J. Nanobiotechnol. 2004, 2, 3.

[31] Stefan Preussler; Hassanain Al-Taiy; Thomas Schneider, Optical spectrum analysis with kHz resolution based on polarization pulling and local oscillator assisted Brillouin scattering, https://ieeexplore.ieee.org/xpl/conhome/7318283/proceeding, https://doi.org/10.1109/ECOC.2015.7341758.

[32] Sztandera, K.; Gorzkiewicz, M.; Klajnert-Maculewicz, B. Gold nanoparticles in cancer treatment. Mol. Pharm. 2019, 16, 1–23. [CrossRef] [PubMed]

[33] Alsultany F. H.; Alhasan S. F. H.; Salim E. T., Seed Layer-Assisted Chemical Bath Deposition of Cu2O Nanoparticles on ITO-Coated Glass Substrates with Tunable Morphology, Crystallinity, and Optical Properties, Journal of Inorganic and Organometallic Polymers and Materials, 31(9), 3749-3759 (2021) 10.1007/s10904-021-02016-y.

[34] Guerrero, E.; Munoz-Marquez, M. A.; Garcia, M. A.; Crespo, P.; Fernandez-Pinel, E.; Hernando, A.; Fernandez, A. Surface plasmon resonance and magnetism of thiol-capped gold nanoparticles. Nanotechnology 2008, 19, 175701.

[35] Fakhri M. A.; Abdulwahhab A. W.; Dawood M. A.; Raheema A. Q.; Numan N. H.; Khalid F. G.; Wahid M. H. A.; Hashim U.; Salim E. T., Optical investigations of nano lithium niobate deposited by spray pyrolysis technique with injection of Li2CO3 and Nb2O5 as raw materials, International Journal of Nanoelectronics and Materials, 11(Special Issue BOND21), 103-108 (2018).

[36] Butet, J.; Brevet, P.-F.; Martin, O.J.F. Optical second harmonic generation in plasmonic nanostructures: From fundamental principles to advanced applications. ACS Nano 2015, 9, 10545–10562.

[37] Doaa A. Mahmoud, Evan T. Salim, Rana O. Mahdi, A. Mindil, Subash C. B. Gopinath & Motahher A. Qaeed, Laser Ablation of Tungsten Metal for Au@WO3 Core-Shell Formation: A Characterizing Study at Different Laser Fluences, Plasmonics (2024). https://doi.org/10.1007/s11468-024-02607-8.

[38] Paul, A., Bhuyan, B., & Dhar, S. S. (2020). Study of core–shell α-Fe2O3@ Au nanohybrid and their high catalytic performances in aerial oxidation of benzyl alcohols. Chemical Engineering Communications, 207(9), 1185-1195.

[39] Doaa A. Mahmoud, Evan T. Salim, Rana O. Mahdi, A. Mindil, Subash C. B. Gopinath & Motahher A. Qaeed, Laser Ablation of Tungsten Metal for Au@WO3 Core-Shell Formation: A Characterizing Study at Different Laser Fluences, Plasmonics (2024). https://doi.org/10.1007/s11468-024-02607-8.

[40] Y. Kamlag, A. Goossens and I. Schoonman, "Laser CVD of cubic SiC nanocrystals", J. of Applied Surface Science, Vol. 184, pp.118-122, 2001.

[41] Azzam Y. Kudhur, Evan T. Salim, Ilker Kara, Makram A. Fakhri & Rana O. Mahdi, Structural optical and morphological properties of copper oxide nanoparticles ablated using pulsed laser ablation in liquid, J Opt 53, 1936–1945 (2024). https://doi.org/10.1007/s12596-023-01331-6.

[42] Fakhri M. A.; Wahid M. H. A.; Badr B. A.; Kadhim S. M.; Salim E. T.; Hashim U.; Salim Z. T., Enhancement of Lithium Niobate nanophotonic structures via spin-coating technique for optical waveguides application, EPJ Web of Conferences, 162, 1004 (2017) 10.1051/epjconf/201716201004.

[43] Mahdi, M. M., Ali, A. M., Alalousi, M. A., Kadhim, D. A., & Abid, M. A. (2024). Developing a copper-zinc-aluminum alloying technique by vacuum thermal deposition after irradiation by gamma rays (NaI (Ti)) with stabilized zinc metal. Vacuum, 219, 112676.

[44] [Azzam Y. Kudhur, Evan T. Salim, Ilker Kara, Makram A. Fakhri & Rana O. Mahdi, Structural optical and morphological properties of copper oxide nanoparticles ablated using pulsed laser ablation in liquid, J Opt 53, 1936–1945 (2024). https://doi.org/10.1007/s12596-023-01331-6.

[45] Fakhri M. A.; Numan N. H.; Mohammed Q. Q.; Abdulla M. S.; Hassan O. S.; Abduljabar S. A.; Ahmed A. A., Responsivity and response time of nano silver oxide on silicon heterojunction detector, International Journal of Nanoelectronics and Materials, 11(Special Issue BOND21), 109-114 (2018).

[46] Zhang, H., Guo, Y., Wu, Z., Wang, Y., Sun, Y., Feng, X., ... & Zhao, G. (2021). Unveiling the theoretical mechanism of purely organic room temperature phosphorescence emission and heteroatomic effects on singlet-triplet intersystem crossing for isopropylthioxanthone derivatives. Journal of Luminescence, 232, 117864.

[47] Tawfiq Z. H.; Fakhri M. A.; Adnan S. A., Photonic Crystal Fibres PCF for Different Sensors in Review, IOP Conference Series: Materials Science and Engineering, 454(1), 12173 (2018) 10.1088/1757-899X/454/1/012173.

[48] Fakhri M. A.; Numan N. H.; Alshakhli Z. S.; Dawood M. A.; Abdulwahhab A. W.; Khalid F. G.; Hashim U.; Salim E. T., Physical investigations of nano and micro lithium-niobate deposited by spray pyrolysis technique, AIP Conference Proceedings, 2045, 20015 (2018) 10.1063/1.5080828.

[49] Krishnan, K. M., Srikrishna, K. V., & Rao, C. N. R. (1997). Nanostructured materials: Grain boundary effects and interfaces. Acta Materialia, 45(2), 729–743. https://doi.org/10.1016/S1359-6454(96)00196-7.

[50] Roaa A. Abbas, Evan T. Salim & Rana O. Mahdi, Morphology transformation of Cu2O thin film: different environmental temperatures employing chemical method, J Mater Sci: Mater Electron 35, 1057 (2024). https://doi.org/10.1007/s10854-024-12823-x.

[51] Mohammed D. A.; Kadhim A.; Fakhri M. A., The enhancement of the corrosion protection of 304 stainless steel using Al2O3 films by PLD method, AIP Conference Proceedings, 2045, 20014 (2018) 10.1063/1.5080827.

[52] Salavati-Niasari, M., Davar, F., & Fereshteh, Z. (2016). Preparation and characterization of gold-decorated α-Fe_2O_3 nanoparticles: Study of morphology and crystal size. Journal of Alloys and Compounds, 654, 52–59.

[53] Jurn Y. N.; Malek F.; Mahmood S. A.; Liu W.-W.; Gbashi E. K.; Fakhri M. A., Important parameters analysis of the single-walled carbon nanotubes composite materials, ARPN Journal of Engineering and Applied Sciences, 11(8), 5108-5113 (2016).

[54] Hassen H. H.; Salim E. T.; Taha J. M.; Mahdi R. O.; Numan N. H.; Khalid F. G.; Fakhri M. A., Fourier transform infrared spectroscopy and photo luminance results for Zno NPs prepared at different preparation condition using LP-PLA technique, International Journal of Nanoelectronics and Materialsm, 11(Special Issue BOND21) 65-72 (2018).

[55] Arif Ullah Khan, Yun Wei, Qipeng Yuan, Kamran Tahir, Zia Ul Haq Khan, Faheem Ullah Khan, Shafiullah Khan, Gul Majid Khan, Farman Ali Khan, Aftab Ahmad, Photocatalytic and antibacterial response of biosynthesized gold nanoparticles, J. Photochem. Photobiol. B Biol. 162 (2016) 273–277.

[56] Evan T. Salim, Ahmed T. Hassan, Rana O Mahdi, Forat H. Alsultany, Physical Properties of HfO2 Nano Structures Deposited using PLD, IJNeaM, vol. 16, no. 3, pp. 495–510, Oct. 2023.

[57] Aseel A. Hadi, Juhaina M. Taha, Rana O. Mahdi, Khawla S. Khashan, Influence of laser pulse on properties of NiO NPs prepared by laser ablation in liquid, AIP Conf. Proc. 2213, 020308 (2020) https://doi.org/10.1063/5.0000115.

[58] Deng, X., & Matranga, C. (2009). Selective growth of Fe2O3 nanoparticles and islands on Au (111). The Journal of Physical Chemistry C, 113(25), 11104-11109.

[59] Zainab T. Hussain, Khawla S. Khashan, Rana O. Mahdi, Characterization of cadmium oxide nanoparticles prepared through Nd:YAG laser ablation process, Materials Today: ProceedingsVolume 42, Pages 2645 – 26482021. https://doi.org/10.1016/j.matpr.2020.12.594.

[60] Fakhri M. A.; Al-Douri Y.; Hashim U., Fabricated Optical Strip Waveguide of Nanophotonics lthium Niobate, IEEE Photonics Journal, 8(2), 7409919 (2016) 10.1109/JPHOT.2016.2531583.

[61] Mahmoudi Alemi, F., Mousavi Dehghani, S. A., Rashidi, A., Hosseinpour, N., & Mohammadi, S. (2021). Potential application of Fe2O3 and functionalized SiO2 nanoparticles for inhibiting asphaltene precipitation in live oil at reservoir conditions. Energy & Fuels, 35(7), 5908-5924.

[62] Fakhri M. A.; Wahid M. H. A.; Kadhim S. M.; Badr B. A.; Salim E. T.; Hashim U.; Salim Z. T., The structure and optical properties of Lithium Niobate grown on quartz for photonics application, EPJ Web of Conferences, 162, 1005 (2017) 10.1051/epjconf/201716201005.

[63] Rana O. Mahdi, Aseel A. Hadi, Juhaina M. Taha, Khawla S. Khashan, Preparation of nickel oxide nanoparticles prepared by laser ablation in water, AIP Conf. Proc. 2213, 020309 (2020) https://doi.org/10.1063/5.0000116.

[64] Braun, S., Bendjus, B., Foltyn, T., Menzel, M., Schreiber, J., & Leson, A. (2004, October). Smoothing of substrate roughness by carbon-based layers prepared by pulsed laser deposition (PLD). In Advances in Mirror Technology for X-Ray, EUV Lithography, Laser, and Other Applications II (Vol. 5533, pp. 75-84). SPIE.

[65] Fakhri M. A.; Al-Douri Y.; Bouhemadou A.; Ameri M., Structural and Optical Properties of Nanophotonic LiNbO3 under Stirrer Time Effect, Journal of Optical Communications, 39(3), 297-306 (2018) 10.1515/joc-2016-0159.

[66] Ismail, R. A., & Abdul-Hamed, R. S. (2017). Laser ablation of Au–CuO core–shell nanocomposite in water for optoelectronic devices. Materials Research Express, 4(12), 125020.

[67] Azzam Y. kudhur, Evan T. Salim, Ilker Kara, Rana O. Mahdi & Raed K. Ibrahim, The effect of laser energy on Cu2O nanoparticles formation by liquid-phase pulsed laser ablation, J Opt 53, 1309–1321 (2024). https://doi.org/10.1007/s12596-023-01319-2.

[68] SHEN, H. X., YAO, J. L., & GU, R. A. (2009). Fabrication and characteristics of spindle Fe2O3@ Au core/shell particles. Transactions of Nonferrous Metals Society of China, 19(3), 652-656.

[69] Khawla S khashan, Rana O Mahdi, Ban A. Badr, Farah Mahdi, Preparation and characterization of ZnMgO nanostructured materials as a photodetector, Journal of Physics: Conference Series 1795 (2021) 012008. doi:10.1088/1742-6596/1795/1/012008

[70] Mahdi, M. M., Salim, E. T., & Obaid, A. S. (2025). A Comparison Study of Au@ Nb2O5 Core–Shell Nanoparticle Using Two Different Laser Flounces. Plasmonics, 1-14.

[71] Roaa A. Abbas, Evan T. Salim & Rana O. Mahdi, Deposition time effect on copper oxide nano structures, an analysis study using chemical method, J Mater Sci: Mater Electron 35, 427 (2024). https://doi.org/10.1007/s10854-024-12143-0.

[72] Cheng, C. W., Sie, E. J., Liu, B., Huan, C. H. A., Sum, T. C., Sun, H. D., & Fan, H. J. (2010). Surface plasmon enhanced band edge luminescence of ZnO nanorods by capping Au nanoparticles. Applied Physics Letters, 96(7).

[73] Jurn Y. N.; Malek F.; Mahmood S. A.; Liu W.-W.; Fakhri M. A.; Salih M. H., Modelling and simulation of rectangular bundle of single-walled carbon nanotubes for antenna applications Key Engineering Materials, 701, 57-66 (2016) 10.4028/www.scientific.net/KEM.701.57.

[74] Bera, A., & Basak, D. (2011). Pd-nanoparticle-decorated ZnO nanowires: ultraviolet photosensitivity and photoluminescenceproperties. Nanotechnology, 22(26), 265501.

[75] Khawla S. Khashan, Aseel A. Hadi, Rana O. Mahdi & Doaa S. Jubair, Aluminum-doped zinc oxide nanoparticles prepared via nanosecond Nd: YAG laser ablation in water: optoelectronic properties, Opt Quant Electron 56, 125 (2024). https://doi.org/10.1007/s11082-023-05630-x.

[76] Banerjee, S., Raja, S. O., Sardar, M., Gayathri, N., Ghosh, B., & Dasgupta, A. (2011). Iron oxide nanoparticles coated with gold: Enhanced magnetic moment due to interfacial effects. Journal of Applied Physics, 109(12).

[77] Abdul Muhsien M.; Salem E.T.; Agool I.R., Preparation and characterization of (Au/n-Sn O2 /Si O2 /Si/Al) MIS device for optoelectronic application, International Journal of Optics, 2013, 756402 (2013) 10.1155/2013/756402.